Capillary based Li-air batteries for in situ synchrotron X-ray powder diffraction studies

Storm, Mie Møller; Johnsen, Rune E.; Younesi, Reza; Norby, Poul

Published in:
Journal of Materials Chemistry A

Link to article, DOI:
10.1039/c4ta04291c

Publication date:
2015

Document Version
Peer reviewed version

Capillary based Li-air batteries for *in situ* synchrotron X-ray powder diffraction studies

Mie Møller Storm, Rune E. Johnsen, Reza Younesi and Poul Norby
Department of Energy Conversion and Storage, Technical University of Denmark, Frederiksborgvej 399, DK-4000 Roskilde, Denmark

Abstract

For Li-air batteries to reach their full potential as energy storage system, a complete understanding of the conditions and reactions in the battery during operation is needed. To follow the reactions *in situ* a capillary-based Li-O_2 battery has been developed for synchrotron-based *in situ* X-ray powder diffraction (XRPD). In this article, we present the results for the analysis of 1st and 2nd deep discharge and charge for a cathode being cycled between 2 and 4.6 V. The crystalline precipitation of Li_2O_2 only is observed in the capillary battery. However, there are indications of side reactions. The Li_2O_2 diffraction peaks grow with the same rate during charge and the development of the full width at half maximum (FWHM) is *hkl* dependent. The difference in the FWHM of the 100 and the 102 reflections indicate anisotropic morphology of the Li_2O_2 crystallites or defects along the *c*-axis. The effect of constant exposure of X-ray radiation to the electrolyte and cathode during charge of the battery was also investigated. X-ray exposure during charge leads to changes in the development of the intensity and the FWHM of the Li_2O_2 diffraction peaks. The X-ray diffraction results are supported by *ex situ* X-ray photoelectron spectroscopy (XPS) of discharged cathodes to illuminate non-crystalline deposited materials.

Introduction

Li-air (Li-O_2) batteries have a theoretical specific energy density comparable to the efficient gravimetric energy density of gasoline, which make them an ideal energy source for battery driven electric vehicles[1]. In the Li-air battery, Li-ions react with oxygen from the air causing precipitation of Li_2O_2 on the air-cathode. The air-cathode is often carbon-based as carbon gives the opportunity to have a light-weight, conducting, and porous cathode. Cathodes based on reduced graphene oxide have demonstrated Li-air batteries with very high capacities[2-4]. However, many challenges are still unsolved for the Li-air battery. Different side reactions take place in the battery and the electrolyte as well as the

cathode have been found to decompose in the oxidizing environment[5-9]. The Li-air battery furthermore has a high overpotential and challenges in regards to cyclability[1]. Several studies show the possibility for a future development of the Li-air battery: Shui et al. [10] demonstrated a capacity limited battery cycled 150 times and theoretical studies shows the possibility of lowering the overpotential for the reversible precipitation of Li_2O_2[11]. The many challenges may be overcome if a clear picture of the conditions and reactions in the battery during operation is obtained. *In situ* studies provide an opportunity to explore systems with a minimum of external interference. Investigation of the cathode and anode materials during discharge and charge is of importance, as these components may hold the key to making a rechargeable Li-air battery with high capacity.

Different designs for *in situ* X-ray diffraction (XRD) studies of Li-air batteries have been explored; Lim et al. [12] designed a battery setup with Li metal on a stage and a cathode separated by a glass fiber separator assembled within a flow chamber with X-ray transparent windows. Ryan et al. [13] performed *in situ* XRD on a Li-O_2 coin cell. The coin cell was set up with Kapton windows within a Kapton sealed flow box. A cell-design based on a Swagelok cell was developed by Shui et al. [14] who investigated the capacity limited discharge/charge on a cell containing Li metal, glass micro-fiber filter, and cathode encapsulated in tubular glass.

Capillary-based batteries for *in situ* X-ray powder diffraction (XRPD) analysis have been used for investigation of Li-ion batteries[15], but no Li-air capillary batteries have yet been designed. We have developed a Li-O_2 capillary battery consisting of an electrolyte filled capillary with anode and cathode in each end coated on stainless steel wires. The oxygen in-let is placed on the cathode-side with a flushing system placed above the capillary. In this study, we present a flexible design of a capillary Li-O_2 battery with discharge and charge investigated using synchrotron-based XRPD. Pure oxygen gas was used as even small amount of impurities as for example CO_2 affects the battery performance[16]. The capillary batteries are therefore termed Li-O_2 batteries in this paper.

In situ XRPD during 1st and 2nd discharge/charge (between 2- 4.6 V) of different battery cells were performed. The effect of X-ray exposure during charging of Li-O_2 batteries was investigated and cathodes deep discharged 1 and 2 times were analyzed *ex situ* with X-ray photoelectron spectroscopy (XPS) to obtain a complete view of the reactions taking place at the air electrode.

Results and Discussion:

This section will start with an introduction to the capillary battery set up and general abilities of the capillary batteries. This is followed by a presentation of the *in situ* XRPD tested batteries (battery 1, 2 and 3), and the XRPD results obtained. The *in situ* results will be followed by a presentation of the *ex situ* XPS analysis of the deeply discharged carbon cathodes.

Figure 1 shows the Li-O_2 capillary cell design, (a picture of the actual Li-O_2 capillary battery is shown in Figure S1). The cathode is mounted on a stainless steel (SS) wire in a quartz tube opposite a Li-anode likewise on a SS wire. Quartz tubes were used for XRPD *in situ* measurements and boro silicate capillaries were used for battery tests without X-ray analysis. Both the cathode and the anode were completely covered by electrolyte and the oxygen was flushed through the flushing unit (Swagelok fitting, drawn in black) to fill the battery with gas. OCV was being measured for 2-3 h before the batteries was cycled between 2-4.6 V.

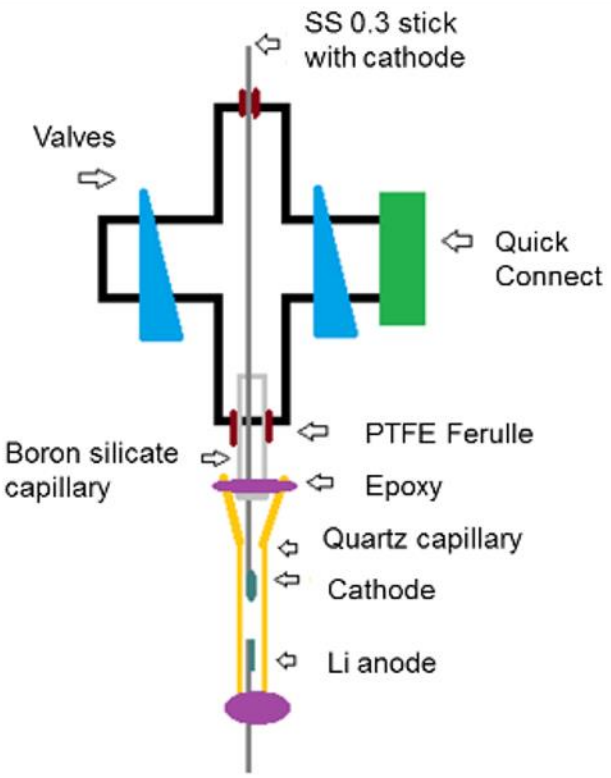

Figure 1: A schematic drawing of Li-O_2 capillary battery for *in situ* XRPD analysis

The *ex situ* batteries had the first discharge plateau around 2.5-2.6 V and a second flat discharge plateau at slightly higher voltage, around 2.7-2.8 V, see Figure 2. The capillary batteries could be cycled between 2 and 4.6 V up to 7 cycles and still maintain a significant capacity, approximately up to 80% of initial discharge capacity.

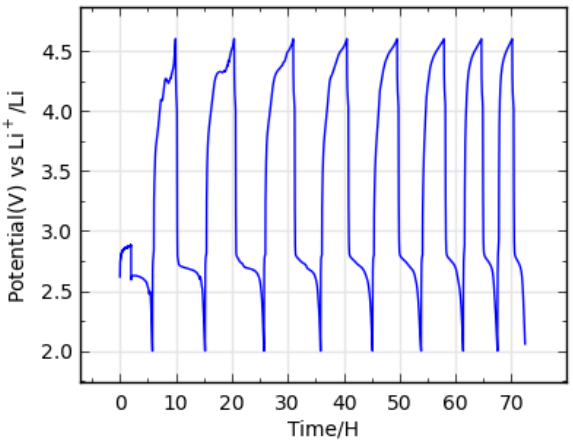

Figure 2: Cycling curves of a Li-O_2 capillary battery upon deep cycling test.

An *ex situ* XRPD measurement of a discharged cathode showed the presence of Li_2O_2 and confirmed the operation of the Li-O_2 battery. Several other studies have shown that deeply discharged Li-air batteries loose capacity upon cycling and that the electrolyte and/or carbon cathode decomposes to different carbonate species[17, 18]. This was confirmed by *ex situ* XRPD measurements of a 5 times discharged cathode which revealed no Li_2O_2 but only other crystalline materials, among those Li_2CO_3, see Figure S2.

Battery 1 was discharged and charged, as shown in Figure 3, at different current rates with XRPD measurements performed every 10 min (30 seconds exposure). The discharge and charge curves were noisy and many spikes were observed under the test run, probably due to insufficient connections between the battery and the potentiostat.

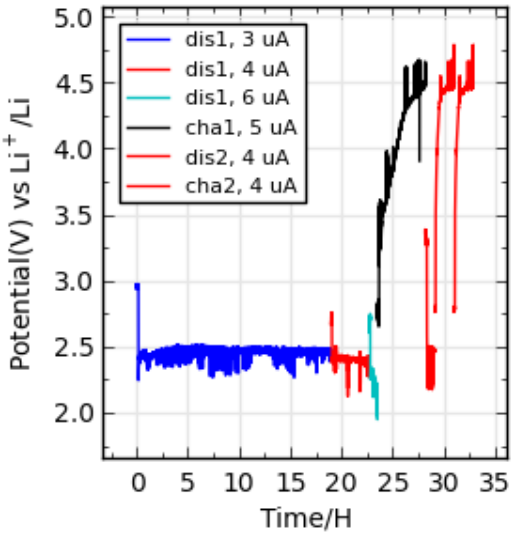

Figure 3: Discharge-charge curve of Li-O_2 capillary battery number 1 for *in situ* analysis.

Figure 3 also show a small second discharge plateau for battery 1. No changes were observed in the intensity or the FWHM of the diffraction peaks during this second discharge and it is not included in the analysis of battery 1. Battery 2 was discharged without exposure to X-ray, and charged with XRPD measurements performed every 10 min, followed by charge with constant exposure to X-ray. Battery 3 was discharged and charged without X-ray radiation, which was followed by analysis of the 2nd discharge/charge cycle with X-ray exposure every 10 min. An overview of the test condition for the batteries is presented in Table 1, further description is given in the experimental section.

Table 1: An overview of the tested batteries

Name	***In situ* battery test**	**Pretreatment without X-ray**
Battery 1	Discharge, charge 1, discharge (negligible) and charge 2	Equilibrated at OCV
Battery 2	Charged with 10 min X-ray exposure every 10 min followed by charging at constant X-ray exposure	Equilibrated at OCV and Discharged
Battery 3	2nd discharge and charge	Equilibrated at

		OCV, discharged and charged

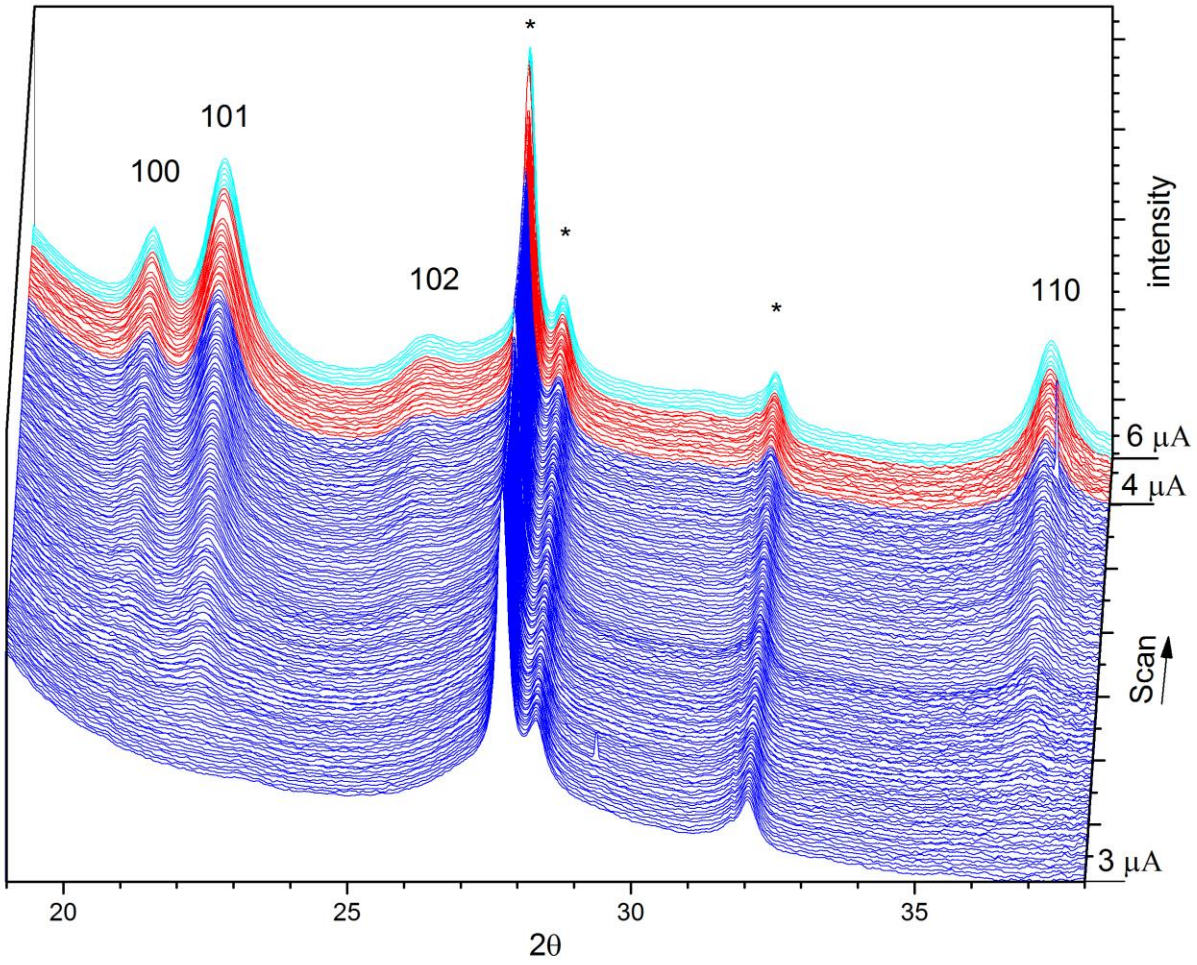

Figure 4: *In situ* diffraction patterns for the discharge of battery 1 showing the appearance of four diffraction peaks of Li_2O_2 and the ones of the SS wire (*). Blue represent a discharge current of -3 µA, red=-4 µA and light blue= -6 µA.

The *in situ* XRPD patterns collected during the discharge of battery 1 are displayed in Figure 4. Capillary battery 1 was discharged for a total of approximately 76 µAh and charged for 32 µAh. Four different Li_2O_2 peaks were observed, the 100, 101, 102, and 110 (21.1°, 22.4°, 26.0°, and 37.0°)

reflections. The diffraction peaks at 27.8°, 28.4°, and 32.1° were caused by the steel wire. Figure 5 shows the area (integrated intensity) of Li_2O_2 100 diffraction peak vs. capacity. The curve appears linear, as seen in Figure 5 for the 100 diffraction peak (the data for the other diffraction peaks can be seen in Figure S3) which could indicate that no side reactions take place during the first discharge. When the areas of the diffraction peaks are normalized the slopes of the different diffractions are of similar values. However, extrapolation of the curves do not cross the origin (crosses y=0 at 0.013 (100), 0.002 (101), 0.012 (102), and 0.019 mAh (110)), and this indicates that some of the electrons in the battery take part in a different reaction than the Li_2O_2 formation.

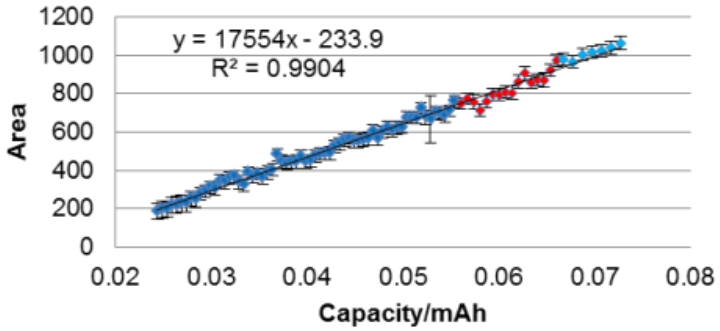

Figure 5: The development of the peak area of the 100 diffraction peak as a function of capacity. Dark blue equals a current of -3 μA, red=-4 μA and light blue= -6 μA.

The slope of the integrated area vs time (not shown here) of the 100, 101 and 110 Li_2O_2 diffraction peaks increased proportionally with increasing discharge rate as expected, as increased current leads to increased Li_2O_2 deposition, as can be seen from Figure 5 and S3 no change in the slope is observed in the area vs. capacity plot. The increase in discharge rate changed neither the battery voltage plateau nor the type of product being deposited. No other discharge products were observed during the test of battery 1.

The charge of battery 1 revealed a decrease of intensity of the Li_2O_2 diffraction peaks for each of the separate charges. The results of area vs. capacity for the first charge are shown in Figure S4. The curves showed that the charge of the battery was slower than the discharge, as we for approximately a third of the charged capacity only observed a decrease in Li_2O_2 intensity of approximately 10 – 20%. This could be caused by possible side reactions probably taking place at the high voltage. It was not

possible to charge the battery completely since the connection in the battery was lost due to the formation of gas bubbles between the cathode and anode.

During discharge the FWHM of the growing 100 diffraction peak decreased, as did the FWHM of the 101 diffraction peak. The plots of the FWHM vs. capacity can be seen in Figure S5 for discharge and S6 for charge. The FWHM of the 102 and 110 diffraction peaks seem to be constant. However, the uncertainty of the parameters was higher as the intensity of these reflections was lower and the FWHM could only be determined in the last part of the discharge. The behavior of the FWHM during charging of battery 1 was more difficult to determine, but if one sees charge 1 and 2, as defined in Figure 3, as a collected series, the FWHM of 100 diffraction peak increased upon charge as did the FWHM of 101 diffraction peaks. The FWHM development of the 100 and 101 diffraction peaks indicate crystallite growth in these directions upon discharge. The development of the FWHM of the 102 and 110 diffraction peaks was not conclusive.

The FWHM values of the 101 and 102 diffraction peaks were higher than those of the 100 and 110 diffraction peaks. This could indicate anisotropic morphology of the Li_2O_2 crystallites or defects along the *c*-axis.

Capillary battery 2 was discharged without exposure to X-ray for 5 h/ -5 µA yielding two different stages, the first being a plateau at the expected voltage for a Li-O_2 battery with a voltage of 2.54 V and the second stage showing a decrease in voltage from 2.2-2.0 V, see Figure S7. The *in situ* charge was initiated by measurements every 10 min and later changed to being at constant X-ray exposure and scans of 30 seconds, see Figure 6.

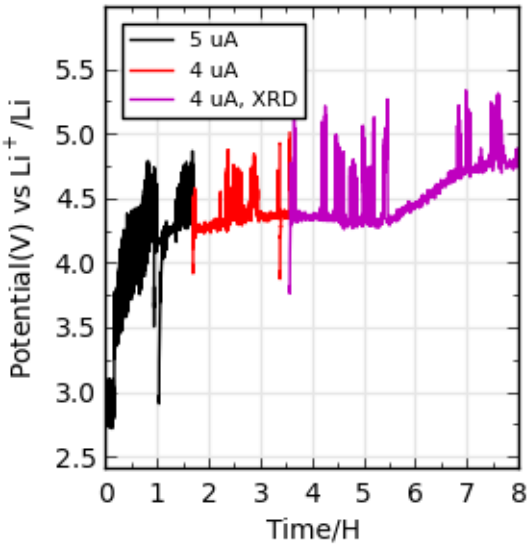

Figure 6: The charge curve of battery 2 under *in situ* XRPD measurements.

The battery reached a voltage plateau around 4.4 V during charge followed by a voltage increase, possibly caused by the depletion of precipitated material. Battery 2 was discharged for approximately 25 µAh and charged for approximately 23.5 µAh before the voltage increase. The results of the *in situ* measurements are shown in Figure 7, which shows both the 10 min measurements (black and red) and the results for the constant X-ray exposure (purple).

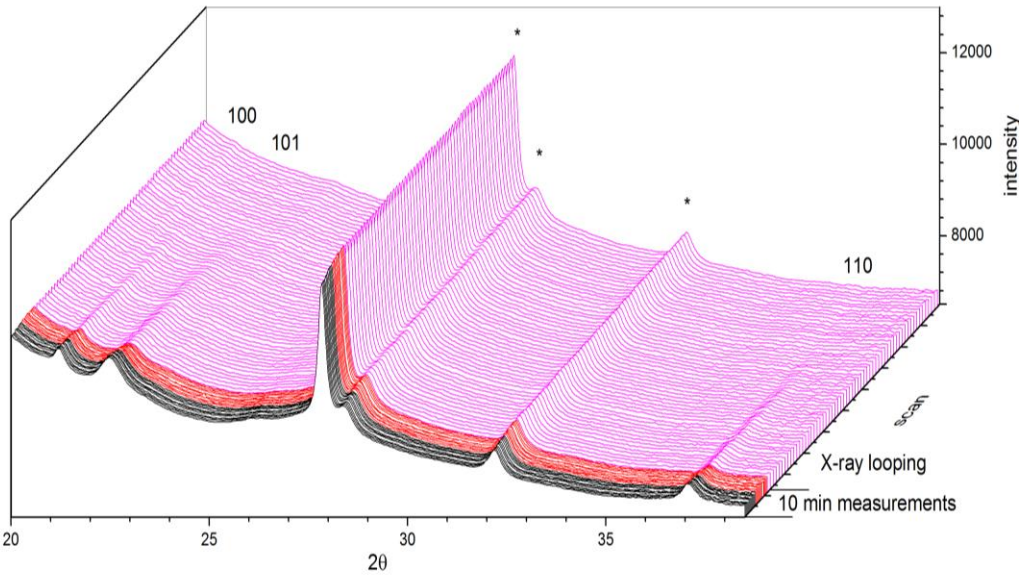

Figure 7: The *in situ* results for the charge of battery 2, showing the decomposition of the three Li_2O_2 diffraction peaks and the SS wire(*). Black = measurements performed every 10 minutes at 5 μA, red = measurements performed every 10 minutes at 4 μA, purple= continuous data collection during X-ray exposure at 4 μA. Only the first 80 constant exposure X-ray scans (2.7 mAh) are displayed in the figure to make it visually easier to read, even though the decomposition of the peaks was observed for longer time.

The XRPD of battery 2 showed the presence of two additional unidentified diffraction peaks at 20.7 and 23.1°, beside the 100, 101 and 110 Li_2O_2 diffraction peaks. These small peaks were not observed in the other *in situ* batteries. Both peaks were very small and had almost constant intensity and FWHM during the charging both with and without constant X-ray exposure. With charging the intensity of all three Li_2O_2 diffraction peaks decreased.

During the 10 min measurements, the rate of the scan was changed from 5 to 4 μa. The *in situ* XRPD measurements during constant X-ray exposure also showed a decomposition of Li_2O_2, see Figure S8. If we assume a linear decomposition of Li_2O_2, the decomposition rate increased by a factor of three for the 100 and 101 diffraction peaks when exposed to X-ray. The decomposition rate for the 110 diffraction peak increased only slightly with the constant X-ray exposure. However, care must be taken when making definite conclusion based on this data, since the 110 diffraction peak was of less intensity

than the other reflection and thus more difficult to analyze. The 100 and 101 diffraction peaks indicate a large enhanced decomposition upon exposure to X-ray radiation.

The FWHM of the 100 diffraction peak increased with charge as did the FWHM of the 101 diffraction peak. This trend matches the one found for battery 1. The FWHM of the 110 diffraction peak in battery 2 decreased with charge, see Figure S9. The broadening of the 100 and 101 increased drastically during the measurements made at constant X-ray exposure, see Figure 8 for the FWHM of the 101 diffraction peak vs. capacity, as did the sharpening for the 110 diffraction peak. This very steep increase only sligthly resembles that of the FWHM for the 100 and 101 diffraction peaks in battery 1 and it does not resemble the development of the 110 diffraction peak. This indicate that the constant X-ray exposure alters the FWHM development for all three diffraction peaks. Along with the drastic development of the area vs. capacity for the 100 and 101 difraction peak this display an effect of the constant X-ray exposure on the Li_2O_2. An accelerated electrochemical decomposition of Li_2O_2 by X-ray during charging was observed by Liu et al[19] who detected decomposition of Li_2O_2 in a Li-air battery fabricated with a porous Li_2O_2 electrode in propylene carbonate electrolyte. The capillary battery results support the observation of increased Li_2O_2 decomposition by X-ray for reactions in dimethoxyethane (DME), and make it clear that the enhanced decomposition also is observed for Li_2O_2 which has been precipitated electrochemically during "normal" Li-O_2 battery discharge.

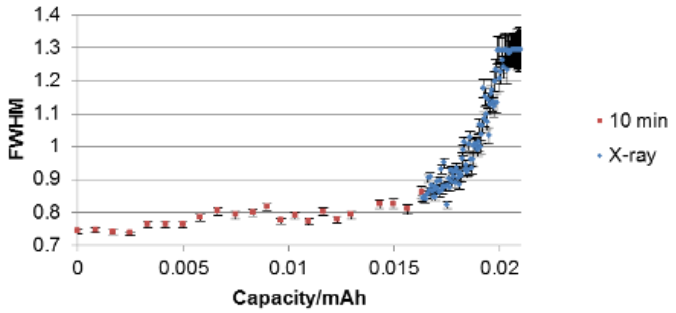

Figure 8: The development of the FWHM for the 101 diffraction peak during charge for battery 2 with and without constant X-ray exposure.

Battery 3 was studied *in situ* during the the 2nd discharge/charge cycle, see Figure S10 for the discharge/charge plots of battery 3. The diffraction peaks of this battery had much lower intensity

compared to those of battery 1 and 2. However, the apperence and disapperence of a small 101 Li_2O_2 diffraction peak upon discharge was observed. No other diffraction peaks were observed for this battery. Whether the lack of intensity for the Li_2O_2 was due to the beam placement in the battery combined with the sligthly smaller slit size or the formation of less Li_2O_2 cannot be determined by diffraction alone, and *ex situ* XPS was performed on discharged cathodes. As the diffraction patterns are of low intensity no further analysis have been performed.

Ex situ XPS analysis was performed on cathodes deep discharged 1 or 2 times to investigate possible changes in the Li_2O_2 precipitation upon battery cycling. The O1s spectra of the discharged and stored cathodes, together with the peak assignments according to the references[20-23], are displayed in Figure 9. The spectra indicate contributions from different oxygen-containing compounds such as Li_2O_2, carbonates, lithium bis(trifluoromethanesulfonyl)imide (LiTFSI) salt, and ethers/alkoxides at binding energies of 531.6, 532.3, 533, and 533.8 eV, respectively (there is also a small peak at very high binding at about 534.7 eV suggesting O bonded to highly electronegative elements such as F). For the "1st discharge" sample, the shoulder at the lower binding energies reveals the presence of Li_2O_2 after 1 discharge, which is in agreement with the *in situ* XRPD results. The relative contribution of Li_2O_2 peak to the O1s spectra decreases from 14% to 4% from the 1st to the 2nd discharge samples. This implies that less Li_2O_2 formed on the 2nd discharge sample. The O1s spectrum of "2nd discharge" sample also shows increased contributions from single- and double-bonded oxygen to carbon indicating increased side products formed by decomposition of the electrolyte. The C1 spectra of the discharge samples (see Figure S11) confirm increased contribution from decomposition products when discharging the electrodes for the 2nd time.

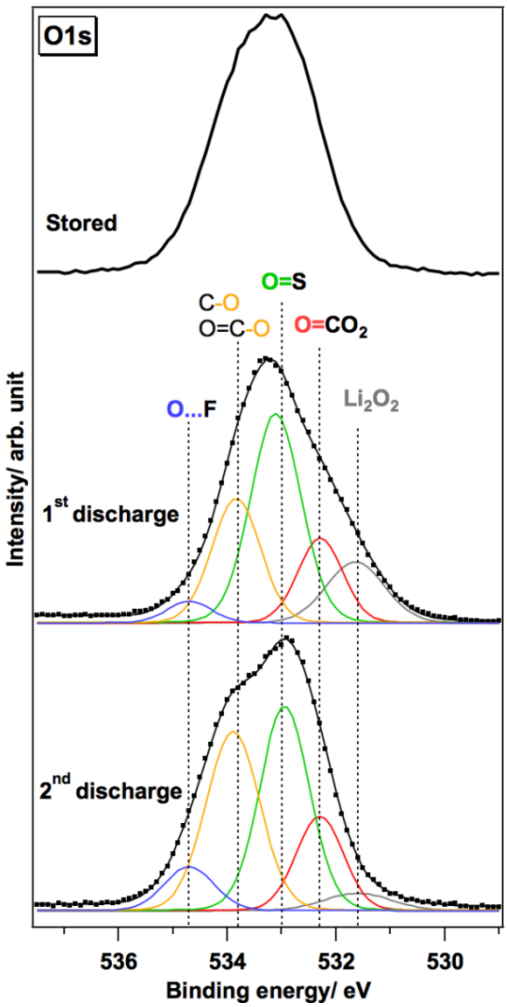

Figure 9: O1s spectra of *ex situ* analyzed cathodes after 1 or 2 discharge together with stored cathode.

The XPS result, which is disclosing smaller amount of Li_2O_2 while higher amount of side products on the 2nd discharge sample compared to the 1st discharge sample, could explain the low intensity of the diffraction peaks of Li_2O_2 observed for the *in situ* XRPD of the 2nd discharge/charge for battery 3.

Experimental

Battery assembly: Figure 1 shows The Li-O_2 capillary cell design. The cathode was made by dip-coating hollow stainless steel (SS) wires (outer diameter 0.3 mm), in a slurry of Super C65 (carbon black from TIMCAL Graphite and Carbon) and 20 wt% polyvinylidene fluoride (PVDF) in N-methyl-2-pyrrolidome (NMP) for *in situ* studies and 15-20 wt% PVDF for *ex situ* studies. The slurry used for

the cathode in battery 3 contained trace amount of diamond powder to facilitate easy alignment of the battery in the X-ray beam. The small carbon cathode was coated at the end of the SS-wire (which had been slightly sanded and cleaned in acetone before use) by dipping the SS-wire in the slurry and drying the slurry with a heating gun at 100 – 110 °C. This process was repeated until a cathode of a sufficient size was made. The cathode stick was dried in vacuum oven inside a glovebox at 80° C for 12 h. The carbon cathodes for the *in situ* study had an average weight of 0.2 mg and the cathodes for the studies of batteries without X-ray and the cathodes for the XPS analysis had an average weight between 0.1-0.2 mg. The Li-anode was prepared by smearing Li onto a 0.4 mm SS-wire which then was glued into a capillary using two-component epoxy. Borosilicate capillaries with an outer diameter of 1.05 mm were used for the *ex situ* XRPD tests, whereas 1 mm quartz capillaries were used for *in situ* XRPD measurements. The quartz capillaries were prepared with a Li-anode in one end and a piece of borosilicate capillary (1.05 mm diameter) in the other end in order to attach it easily to the Li-O_2 flushing unit. The flushing unit had two valves with a quick connector in one end for the inlet of oxygen. The carbon cathode was attached to the unit with a Teflon ferrule and the capillary was filled with 1M LiTSFI in DME electrolyte and attached to the unit with a Teflon ferrule. Both the anode and cathode were covered by the electrolyte. The two Teflon ferrules hinder short circuiting the battery. The Li-O_2 capillary batteries were assembled inside a glovebox and were tightly sealed before removal from the glovebox. The batteries were flushed several times with oxygen gas (grade 5.0) which resulted in an overpressure of approximately 1.5-2 bars inside the batteries. The valves ensured that the capillary unit could be moved around with the flushing unit working as an oxygen reservoir. The air-exposed end of the capillary coated SS-wire was carefully sealed with two component epoxy glue before the oxygen activation process. Small additional wires were attached to the anode and cathode side of the battery for attaching the potentiostat to the *in situ* setup.

Battery tests: Several capillary-based batteries were electrochemically tested using a Biologic potentiostat and EC-lab software. To analyze formation and decomposition of Li_2O_2 in Li-O_2 cells, three different cells were used in the *in situ* synchrotron-based XRPD experiments. The batteries for *ex situ* XRPD and XPS analysis were left after oxygen filling for 2- 3 h. at OCV before being discharge/charged at -/+ 3 µA to 2 V/ 4.6 V. The *in situ* battery 1 was activated for approx. 5 h., followed by a discharge at -3 µA for 18 h 48 min, a discharge at - 4 µA for 3 h. 45 min, and a final discharge at -6 µA. The battery was charged at 5 µA and discharged for a second time at 4 µA for 1 h,

before being recharged at 4 µA (as seen in Figure 2). The XRPD patterns of the cathode were collected every 10 min with an exposure time of 30 s. The voltage of the first discharge at 3 µA have been smoothed using Origin Pro 8.6, using the Adjacent-Avarage signal process. The second discharge of battery 1 was short, 1 h, and no changes in the area of the diffraction peaks or FWHM were observed probably due to the short duration of the discharge, and the data is not presented in this paper.

After 3 h of resting time at OCV battery 2 was discharged without being exposed to X-ray radiation at 5 µA to 2 V. It was then charged *in situ* with XRPD measurements every 10 min and 30 s exposure time, at 5 µA for 100 min and at 4 µA for 110 min. The battery was charged at 4 µA with continuous exposure to X-ray for approximately 6.6 h. Similar to battery 1, battery 2 gave a noisy battery test curve, which was restarted three times due to voltage spikes.

Battery 3 was kept at OCV for 3 h before battery discharge and charge without X-ray exposure at 4 µA. The 2nd discharge-charge was performed *in situ* with XRPD patterns being collected every 10 min with an exposure time of 60 s. The battery was discharged at -5 µA for 100 min followed by a discharge and charge at -/+6 µA.

XRPD: Beamline I711 at MAX-lab was used for the XRPD measurements for battery 1 and 2 with a wavelength of 0.9940 Å, a detector distance of approximately 96 mm and a slit size of 0.2*0.2 for the batteries. Between the XRPD measurements the shutter was closed in order to minimize any radiation-induced degradation of the sample. The data were integrated by Fit2D [24], normalized to the background and fitted in Topas3 [25] as single pseudo-Voigt peaks and a background described by a 5th order Chesbyschev function. Battery 3 was measured at the ESRF at the Swiss Norwegian beamline with a wavelength of 0.7735 Å, a distance to the detector of approximately 194 mm and a slit size of 0.15*0.15. *Ex situ* XRPD was measured with a BrukerD8 using CuKα radiation.

XPS: Before *ex situ* analysis by XPS, the capillary batteries discharged one and two times, respectively were carefully disassembled in the glovebox, and the cathodes were washed with dried DME and left for drying. A background sample was stored in electrolyte overnight inside the glovebox before being washed and sealed under similar conditions as the discharged cathodes. The XPS samples were prepared in glovebox on Cu-tape and transported to the XPS machine inside an airtight transfer chamber. XPS measurements were performed on a commercial in-house PHI 5500 spectrometer with monochromatic Al Kα radiation. Scans were made with a step size of 0.1 eV and 35 to 50 repeated cycles. Igor Pro [26] was used for spectral analysis.

Conclusion

The *in situ* XRPD analysis of the cathodes of Li-O_2 capillary batteries revealed precipitation of Li_2O_2 by the growth of the 100, 101, 102 and 110 diffraction peaks upon discharge. Only the Li_2O_2 diffraction peaks were affected by the discharge/charge of the *in situ* analyzed batteries. The development in the FWHM indicated growth in the crystallite size, as seen by narrowing of the 100 and 101 diffraction peaks upon discharge. A constant exposure to X-ray during charge, increased the decomposition rate of the 100 and 101 diffraction peaks remarkable, compared to a small increase for the 110 diffraction peak. The development of the FWHM upon constant X-ray exposure was dramatically and could indicate that X-ray exposure affects the general Li_2O_2 decomposition. Upon charging of the battery a complete decomposition of Li_2O_2 was observed. The 2nd discharge/charge showed a single very low intensity Li_2O_2 diffraction peak which together with the XPS results indicated a decrease in Li_2O_2 precipitation upon deep discharged cycling.

Acknowledgement

The authors acknowledge support from University of Uppsala, Department of Chemistry - Ångström Laboratory, Structural Chemistry, Prof. Kristina Edström and the MAX-lab staff at beam-line I711. Further acknowledgement is given to the ESRF staff at the Swiss-Norwegian beam-line, the ReLiable project funded by the Danish Council for Strategic Research−Programme Commission on Sustainable Energy and Environment (project no. 11-116792), and The Danish Research Council for the financial support of synchrotron measurements (DANSCAT).

References

1. G. Girishkumar, B. McCloskey, A. C. Luntz, S. Swanson and W. Wilcke, *J. Phys. Chem. Lett.*, 2010, **1**, 2193-2203.
2. J. Xiao, D. Mei, X. Li, W. Xu, D. Wang, G. L. Graff, W. D. Bennett, Z. Nie, L. V. Saraf, I. A. Aksay, J. Liu and J.-G. Zhang, *Nano Lett.* , 2011, **11**, 5071-5078.
3. Y. Li, J. Wang, X. Li, D. Geng, R. Li and X. Sun, *Chem. Commun.*, 2011, **47**, 9438-9440.
4. M. M. Storm, M. Overgaard, R. Younesi, N. E. A. Reeler, T. Vosch, U. G. Nielsen, K. Edström and P. Norby, *Carbon*, 2014, submitted.

5. B. D. McCloskey, D. S. Bethune, R. M. Shelby, T. Mori, R. Scheffler, A. Speidel, M. Sherwood and A. C. Luntz, *J. Phys. Chem. Lett.*, 2012, **3**, 3043-3047.
6. M. M. Ottakam Thotiyl, S. A. Freunberger, Z. Peng and P. G. Bruce, *J. Am. Chem. Soc.*, 2013, **135**, 494-500.
7. M. Balaish, A. Kraytsberg and Y. Ein-Eli, *Phys. Chem. Chem. Phys.*, 2014, **16**, 2801-2822.
8. R. Younesi, P. Norby and T. Vegge, *ECS Electrochem. Lett.* , 2014, **3**, A15-A18.
9. R. Younesi, *University of Uppsala Ph.D. thesis*, 2012, Characterization of Reaction Products in the Li-O2 Battery Using Photoelectron Spectroscopy.
10. J. Shui, F. Du, C. Xue, Q. Li and L. Dai, *ACS Nano*, 2014, **8**, 3015-3022.
11. J. S. Hummelshøj, J. Blomqvist, S. Datta, T. Vegge, J. Rossmeisl, K. S. Thygesen, A. C. Luntz, K. W. Jacobsen and J. K. Nørskov, *J. Chem. Phys*, 2010, **132**, 071101.
12. H. Lim, E. Yilmaz and H. R. Byon, *J. Phys. Chem. Lett.*, 2012, **3**, 3210-3215.
13. K. R. Ryan, L. Trahey, J. S. Okasinski, A. K. Burrell and B. J. Ingram, *J. Mater. Chem. A*, 2013, **1**, 6915-6919.
14. J.-L. Shui, J. S. Okasinski, P. Kenesei, H. A. Dobbs, D. Zhao, J. D. Almer and D.-J. Liu, *Nat Commun*, 2013, **4**.
15. R. E. Johnsen and P. Norby, *J. Appl. Crystallogr.*, 2013, **46**, 1537-1543.
16. Y. S. Mekonnen, K. B. Knudsen, J. S. G. Mýrdal, R. Younesi, J. Højberg, J. Hjelm, P. Norby and T. Vegge, *J. Chem. Phys*, 2014, **140**, -.
17. M. M. O. Thotiyl, S. A. Freunberger, Z. Q. Peng and P. G. Bruce, *J. Am. Chem. Soc.*, 2013, **135**, 494-500.
18. B. D. McCloskey, D. S. Bethune, R. M. Shelby, G. Girishkumar and A. C. Luntz, *J. Phys. Chem. Lett.*, 2011, **2**, 1161-1166.
19. J. Liu, M. Roberts, R. Younesi, M. Dahbi, K. Edström, T. Gustafsson and J. Zhu, *J. Phys. Chem. Lett.*, 2013, **4**, 4045-4050.
20. R. Younesi, M. Hahlin, M. Roberts and K. Edström, *J. Power Sources*, 2013, **225**, 40-45.
21. R. Younesi, M. Hahlin, F. Björefors, P. Johansson and K. Edström, *Chem. Mater.*, 2012, **25**, 77-84.
22. Y.-C. Lu, A. N. Mansour, N. Yabuuchi and Y. Shao-Horn, *Chem. Mater.*, 2009, **21**, 4408-4424.
23. S. Leroy, H. Martinez, R. Dedryvère, D. Lemordant and D. Gonbeau, *Appl. Surf. Sci.*, 2007, **253**, 4895-4905.
24. A. P. Hammersley, *ESRF Internal Report* 1997, **ESRF97HA02T**.
25. Topas3, *BRUKER-AXS*, 2000.

26. IGORPro, *WaveMetric*, Version 4.0